

# A New Method for Nearly Automated Detection of Carotid Contours on Ultrasound Images Based on Combined Region Growing and Level-Set

EG Caiani<sup>1</sup>, C Corsi<sup>2</sup>, P Tombolato<sup>1</sup>, C Lamberti<sup>2</sup>, S Cerutti<sup>1</sup>

<sup>1</sup>Dipartimento di Bioingegneria, Politecnico di Milano, Italy

<sup>2</sup>Dipartimento di Elettronica, Informatica e Sistemistica, Università di Bologna, Italy

## Abstract

We developed a new method for “nearly-automated” carotid (CA) contour detection by combining seeded region growing (SRG) and level-set (LS) methods. This technique was applied to cross-sectional vascular images (Aspen, Siemens) acquired during parabolic flight in 5 normal subjects, to detect carotid area changes with gravity (Gz). For each frame, the region resulting from SRG was used to initialize the LS algorithm. This resulted in the final CA contour, from which its area (CAA) was computed. Three consecutive cardiac cycles were selected and max (MCAA) and min CAA (mCAA), as well as their difference *D*. Compared to 1 Gz, at 0 Gz MCAA was increased by  $11.2 \pm 5.5\%$  ( $p=0.07$ ), mCAA was unchanged and *D* augmented by  $44.8 \pm 7.2\%$  ( $p<0.01$ ). The developed method was able to reliably detect the CA lumen compatibly with image quality. Expected changes due to increased stroke volume at 0 Gz were quantified.

## 1. Introduction

The quantification of the cross-sectional dimensions of the carotid (CA) artery by ultrasound techniques is important to obtain clinical information about cerebral perfusion and the estimate of the cardiac output. In clinical practice, such evaluation is based on the manual tracing of the CA lumen contours, which is time consuming and subjective.

Seeded region growing (SRG) [1-3] and level-set (LS) methods [4-6] are widely used techniques for biomedical image segmentation. However, both SRG and LS have some limitations when applied to ultrasound (US) images. In fact, due to speckle noise, SRG fails in discriminating between the real structure and artefacts with similar characteristics, while LS needs frame-by-frame manual initialization of the initial contour. To overcome the limitations of SRG and LS applied singularly, our aim was to develop a new method by combining SRG and LS techniques for “nearly-automated” CA contour detection. The ability of the proposed technique in detecting

changes in CA lumen dimensions will be tested by the analysis of carotid images acquired during parabolic flight, which is known to induce abrupt changes in blood flow redistribution and stroke volume due to different gravity (Gz) conditions.

## 2. Methods

Parabolic flights were performed in the Zero-G Airbus A-300 (Novespace, CNES-ESA, Bordeaux, France). Each flight campaign consisted in three days of flight, performing in each 31 parabolas. Each parabola included four consecutive phases: normogravity (1 Gz, 1 min); mild hypergravity (1.8 Gz, 20 sec) during the ascending phase of the parabola; microgravity (0 Gz, 24 sec); a second period of mild hypergravity (1.8 Gz, 20 sec) during the descending phase of the parabola. A group of five normal subjects (mean age  $\pm$  SD, 42 age  $\pm$  5 years) was studied in standing upright position. Two-dimensional cross-sectional vascular images, continuously acquired during the parabola (frame rate 16 Hz), were obtained with an Aspen (Acuson, Siemens, France) ultrasound unit at the carotid level, using a vascular probe (5-7 MHz). To test for the effects of different spatial resolution on the algorithm performance, for each subject image acquisition was repeated with different resolution settings: A) 64 pixel/cm<sup>2</sup> and 16 fps; B) 280 pixel/cm<sup>2</sup> and 6 fps. To automatically detect the CA contour, an algorithm based on SRG combined with LS methods was developed (Matlab 6.5, The MatWorks Inc.).

### 2.1. Seeded region growing

First, a border detection algorithm based on quad-tree decomposition and SRG [1] was applied to every frame *n* of the sequence. The image was divided into blocks according to the condition:

$$|\max(I) - \min(I)| \leq \text{threshold} \quad (1)$$

where *I* represents the pixel intensity. The minimum size for each block was set to 2x2 pixels and the optimal threshold value was experimentally determined as equal

to 7/255. Then, the SRG procedure was applied in order to define the homogeneous region  $R_T$  representing the carotid cross-sectional area. For this purpose, an initial seed point was manually located in the centre of the CA lumen on the first frame of the sequence (Figure 1).

Given the seed, SRG determined image tessellation by assuming that each connected component  $(i,j)$  of the region  $R_T$  meets the following homogeneity criterion:

$$|I(i_T, j_T) - I(i, j)| \leq h_n \quad \forall (i, j) \in R_T \quad (2)$$

where  $(i_T, j_T)$  represents the coordinates of the seed point and  $h_n$  is the threshold value for the frame  $n$ .

This criterion allows including in  $R_T$  all connected pixel blocks, obtained by the quad-tree decomposition, which intensity does not differ from the seed point intensity more than a user-defined threshold value  $h_n$  [2].

To optimize the selection of  $h_n$ , the knowledge of the circular shape of the carotid lumen was utilized. Based on this observation,  $h_n$  was defined as a non-linearly decreasing function depending on the distance of the block from the seed point:

$$h_n = \frac{1}{\rho_{n-1} \sqrt{(i - i_T)^2 + (j - j_T)^2}} \quad (3)$$

where  $\rho_{n-1}$  is the mean radius of the CA lumen computed in the previous frame  $n-1$ . In this way, the algorithm would result in a quasi-circular  $R_T$  even in presence of artifacts, such as partial shadowing of the CA contour.

As a result, for blocks closer to the seed, their probability to be included in  $R_T$  will be higher, as evidenced by a high  $h_n$  (Figure 2).

Finally, the perimeter  $P(i,j)$  of the CA lumen was extracted as the boundary of  $R_T$ , and used to initialize the LS algorithm.

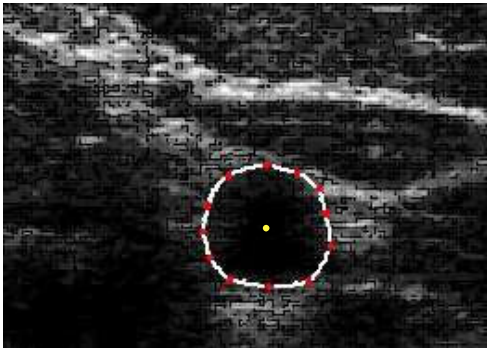


Figure 1. Initialization procedure on the first frame of the sequence. Several points are manually selected in correspondence to the boundary of the CA lumen. Then, a cubic spline is fitted to the points (white line) to obtain a circumference, which center is considered as the initial seed point position.

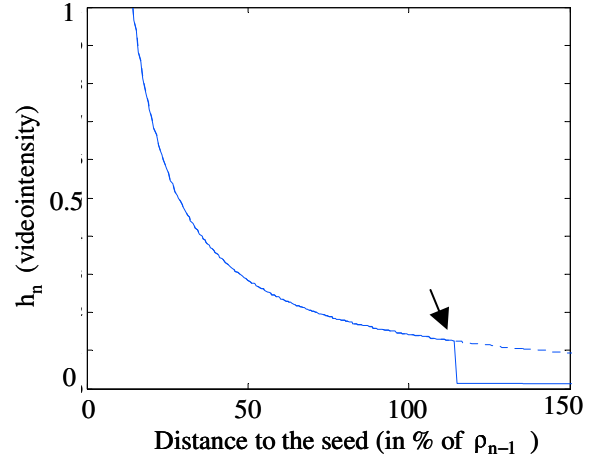


Figure 2. Representation of the non-linearly decreasing threshold  $h_n$  as a function of the normalized distance of the block from the seed. The arrow indicates a discontinuity at 114% introduced to avoid possible expansion of  $R_T$  towards regions too far from the seed point.

## 2.2. Level set methods

The level set approach is an implicit representation of curves, in the form of a partial differential equation (PDE), that tracks boundaries as they evolve in space and time. The detected contour is represented as the zero level set of a higher dimensional function, called level set function  $\phi(x,t)$ , which is embedding it and whose motion is guided by the PDE under the constraints imposed by the problem [5-7]:

$$\frac{\partial \phi}{\partial t} - \alpha g \cdot |\nabla \phi| - \beta \nabla g \cdot |\nabla \phi| + \gamma K \cdot |\nabla \phi| = 0 \quad (4)$$

with the initial condition  $\phi(x,0)=\phi_0$ . The last term represents an interface tension force, controlled by the parameter  $\gamma$  (set to 0.25) and by the curvature  $K = \nabla(\nabla \phi / |\nabla \phi|)$ . The third term describes a force that attracts the level set towards the boundaries, weighted by the parameter  $\beta$  (set to 5) that limits the regularization of the embedding, where the edge indicator  $g$  is a non-increasing function of the gradient of a smoothed version of the initial image [8]:

$$g = \left[ 1 + \left( \frac{|\nabla(G_\sigma \otimes I(x))|}{\alpha} \right)^2 \right]^{-1} \quad \text{with} \quad G_\sigma(\xi) = \frac{1}{\sigma\sqrt{\pi}} e^{-\left(\frac{\xi}{\sigma}\right)^2}$$

The second term is an expansion/contraction term, weighted by  $\alpha$ . The parameter  $\alpha$  (set to 1) selects the contrast of the objects to consider in the image during the motion of the embedding, and the variance  $\sigma$  (set to 0.6) of the Gaussian  $G_\sigma$  defines the size of the smallest detectable features in the image [9].

The segmentation procedure started with the

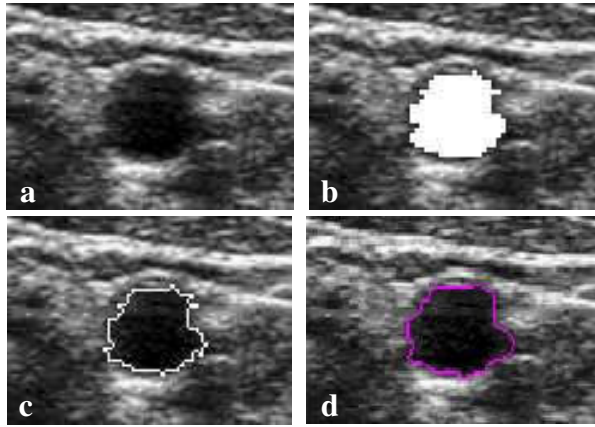


Figure 3. Example of the detection procedure: a) original image; b) homogeneous region as a result of SRG; c) perimeter of the homogeneous region, used as zero level set; d) final contour resulting from the LS algorithm.

initialization of the level set function, to determine  $\phi(x,0) = \phi_0$ . This stage is necessary because the curvature  $K$  in the geometry dependent term and the vector field represented by  $\nabla g$  in the advection term act only close to the object boundary.

The zero level set  $\phi_0$  was defined by the points of the perimeter  $P(i,j)$  resulting from the SRG, joint to define a polygonal contour from which the signed distance function was computed, with negative values inside and positive values outside.

The zero level of the signed distance function evolved under the motion guided by (4) for a fixed number of iterations (set to 30, as a good compromise between computation time, accuracy and stability of contour detection). At the end of this evolution, a contour corresponding to the boundary of the CA lumen was obtained (Figure 3), as the final position of the zero level of the level set function, and its area (CAA) computed.

The whole procedure was then iteratively repeated for the next frame in the sequence, by considering as new seed position for SRG the centre of the detected lumen by LS, and as its videointensity the average of the seeds videointensity in the previous frames.

### 2.3. Carotid area parameters computation

For each subject, from the CAA vs time curves relevant to 1 Gz and 0 Gz, 3 consecutive cardiac cycles were manually selected. For each cycle, the maximum (MCAA) and minimum (mCAA) area were quantified, as well as their difference  $D = MCAA - mCAA$ . Also,  $D\%$  was computed as  $100 * D / MCAA$ . Then, the measurements obtained from each cycle were averaged, to minimize respiratory variations. Differences in the computed parameters between 1 Gz and 0 Gz were tested by paired t-test ( $p < 0.05$  as significant).

## 3. Results

A total of 538 frames was analyzed, with a mean computation time of 1.45 sec/frame and 81 sec/frame for A and B resolution settings, respectively. Once the contour was detected, it was overlaid on the original image to allow visual verification. Moreover, the CA area was computed as pixel counts, and multiplied to the proper scale factor to obtain the CAA in  $cm^2$  (Table 1).

CAA waveforms obtained by images acquired with A resolution settings better reflected the morphology of the carotid pressure signal, due to the higher time resolution.

Compared to 1 Gz, at 0 Gz MCAA was increased by  $11.2 \pm 5.5\%$  ( $p = 0.07$ ), while mCAA was unchanged. As a result,  $D$  and  $D\%$  were increased by  $44.8 \pm 7.2\%$  ( $p < 0.01$ ) and  $30.9 \pm 12.3\%$  ( $p < 0.05$ ), respectively.

Table 1. Mean  $\pm$  SD of absolute measurements (in  $cm^2$ ) of the parameters extracted from the carotid area waveforms vs time.

	MCAA	mCAA	D
1 Gz	$0.320 \pm 0.096$	$0.274 \pm 0.073$	$0.046 \pm 0.027$
0 Gz	$0.406 \pm 0.028$	$0.328 \pm 0.025$	$0.077 \pm 0.024^*$

\*:  $p < 0.05$  paired t-test.

## 4. Discussion and conclusions

To allow the “nearly automated” quantification of the area of the CA lumen from cross-sectional ultrasound sequences, thus reducing the subjectivity of the analysis, we developed a new segmentation technique by combining SRG and LS methods. We chose to utilize this combined approach to overcome the limitations of each technique, when applied alone to this kind of datasets.

The SRG technique identifies the object based on its homogeneous videointensity. This characteristic is useful to identify the CA lumen. However, SRG could fail in the frames when shadowing artefacts are present, and the CA lumen is not completely visualized, or when speckle noise, which affects ultrasound images, prevents the proper detection of discontinuities in videointensity.

On the other hand, the LS technique is able to activate or stop such evolution in presence of artefacts in the image, thus providing a smooth contour of the desired object, less affected by speckle noise. However, in our formulation, this method needs an initialization of the contour as closer as possible to the real one.

In order to reduce manual interaction, we used the contour resulting from the SRG algorithm as LS initialization. In this way, the operator had only to identify few points in correspondence of the CA lumen boundaries on the first frame of the sequence, to properly compute the first seed point position. Then, in the following frames, the results obtained for the previous

frame were utilized to automatically set the new seed point position and videointensity.

In the algorithm implementation, particular care has been given in the definition of the parameters of the two methods, to optimize the reliability of the contour detection. In particular, based on the circularity of the CA lumen, the SRG threshold has been considered as a non linear function, decreasing with the inverse of the distance between the seed and each analyzed block, normalized by the mean radius of the CA lumen in the previous frame. The normalization was introduced to keep the threshold independent from both the spatial image resolution and the CA lumen radius, which could vary between subjects.

In the application of the developed algorithm on ultrasound images acquired during parabolic flight, the resolution settings A were found better than B: in B, the greater precision in area computation implied excessive computational time and loss of morphological characteristics in the CAA waveform. The ability of the algorithm in detecting expected changes in CA dimensions due to changes in preload was verified. In fact, parabolic flight induces abrupt changes in gravity which are known to cause significant modification in venous return, and consequently in left ventricular stroke volume (LVSV).

We previously demonstrated, by real-time three-dimensional echocardiography, that LVSV was increased by 20% at 0 Gz compared to 1 Gz [10]. By the analysis of the CAA versus time curves, we evidenced a substantial, hence not significant, increase between 1 Gz and 0 Gz in the MCAA, following ventricular ejection, probably reflecting an increase in the intra-carotid pressure due to the increased LVSV, thus resulting in a variation of the carotid stiffness. Also, the significant increase in D and D% at 0 Gz reflected the change in LVSV. The increase in D by about 40%, compared to the previously reported increase in LVSV by 20%, could reflect the high redistribution of blood flow in the upper districts with microgravity, which is known to produce facial edema, nasal congestion, headache, and distension of head and neck veins in astronauts during space flight [11].

The proposed method resulted in fast, accurate, nearly automated detection of cross-sectional carotid contours. Such analysis, combined with the Doppler evaluation of the carotid flow velocity, could allow the computation of the carotid flow and thus provide useful information about brain perfusion during different experimental conditions, as well as an indirect estimate of the cardiac output, computed as 3\* carotid flow.

## Acknowledgements

We want to acknowledge Pierre Vaida, Andre Capderou, Suzel Bussieres, Christian Kays, André Technouyers and Bernard Cholley from the Parabolic Flight Team of the University of Bourdeaux 2 “Victor Segalen” for their support and help in the organization of the data acquisition session.

## References

- [1] Adams R, Bischof L. Seeded region growing. *IEEE Trans on Pattern Analysis and Machine Intelligence* 1994;16:641-7.
- [2] Liou Y, Pavlidis T. Enhancements of the split and merge algorithm for image segmentation. *Proc. Robotics and Automation* 1998;3:1567-72.
- [3] Alakuijala J, Laitinen J, Sallinen S, Helminen H. New efficient image segmentations algorithm: competitive region growing of initial regions. *Proc. IEEE-EMBS* 1997;1:409-10.
- [4] Osher S, Sethian JA. fronts propagating with curvature dependent speed: algorithms based on Hamilton Jacobi formulation. *J Computational Physics* 1988;79:12-49.
- [5] Sethian JA. *Level set methods and fast marching methods*. Cambridge: University Press 1999.
- [6] Malladi R, Sethian JA, Vemuri BC. Shape modelling with front propagation: a level set approach. *IEEE Trans Patterns Analysis and Machine Intelligence* 1995;17(2):158-75.
- [7] Corsi C, Saracino G, Sarti A, Lamberti C. Left ventricular volume estimation for real-time three-dimensional echocardiography. *IEEE Trans Med Imaging* 2002;21:1202-8.
- [8] Perona P, Malik J. Scale-space and edge detection using anisotropic diffusion. *IEEE Trans Pattern Analysis and Machine Intelligence* 1990;12:629-639.
- [9] Morel JM, Solimini S. variational methods in image segmentation. In: *Progress in nonlinear differential equation and their applications*. 1995;14, Birkhauser, Boston.
- [10] Caiani EG, Sugeng L, Weinert L, Capderou A, Lang RM, Vaida P. Objective evaluation of changes in left ventricular and atrial volumes during parabolic flight using real-time three-dimensional echocardiography. *J Appl Physiol* 2006;101:460-8. Epub 2006 Apr 6.
- [11] Thornton WE, Hoffler GW, Rummel JA. Anthropometric changes and fluid shifts. In: Johnson RS, Dietlein LF, *Biomedical results from Skylab*. Washington, DC: NASA, 1977:330-338..

Address for correspondence

Dr. Enrico G Caiani  
Biomedical Engineering Department, Politecnico di Milano  
Piazza L. da Vinci 32, 20133 Milano, ITALY  
[caiani@biomed.polimi.it](mailto:caiani@biomed.polimi.it)